Polymer Nanoparticles containing Gold Nanoclusters

Bárbara Casteleiro

CQFM, Instituto Superior Técnico, Universidade de Lisboa, Portugal

Laboratoire d'Ingénierie des Matériaux polymers –UMR CNRS 5223, Université Claude Bernard Lyon1, France

Abstract Gold Nanoclusters (AuNCs) are a unique emerging class of gold particles with a well-defined structure have low toxicity, fluorescence emission. Their characteristics make them attractive for a wide range of applications: catalysis, imaging and sensing. There are still some issues, such as handling and storage, which can be solved by their incorporation into polymer nanoparticles (PNPs). Two techniques were tested: miniemulsion polymerization and polymerization induced self-assembly (PISA). Miniemulsion polymerization is a robust technique widely used for the incorporation of inorganic compounds, while PISA is a new polymerization technique quite versatile and direct. We achieved PNPs incorporating AuNCs by miniemulsion polymerization (diameter about 60 nm) and by PISA (diameter about 30 nm) with emission at 825 nm.

Keywords Gold Nanoclusters, Miniemulsion polymerization, PISA, Gold Nanoclusters stability, hybrid gold-polymer nanoparticles

1. Introduction

Gold Nanoclusters (AuNCs) are known for their optical properties, well-defined structure and organization, having dimensions below 2 nm [1]. They are a structure between atoms and molecules, since they have discrete electronic structure, photoluminescence, HOMO-LUMO transition and intrinsic magnetism [2]. The loss of metallic character leads to the absence of the surface plasmon resonance, since the electrons are localized [3]. Another important feature is the discretization of the energy level due to the quantum confinement, since the AuNCs have a size comparable with the Fermi's wavelength. Other important features of these clusters are long fluorescence lifetime, large Stokes shift, biocompatibility, photostability [4], low toxicity [5] and catalytic activity [2]. They make the AuNCs very attractive for a wide the range of applications.

The band gap size and affinity with stabilizers depend on the number of atoms. Smaller AuNCs have larger band gaps, and emission in the UV range. On the other hand, larger AuNCs have smaller band gaps and consequently emission in the visible and IR range. This can be explained by the discretization of energy levels, which loses importance with the increase in size, leading to smaller band gaps for larger sizes.

Some of the applications of AuNCs include their use as catalysts [5], chemiresistors [6, 7], in imaging[4, 8, 9], for biolabeling [4], in sensing [4, 10, 11] and in theranostics [12-15]. Their applications depend on their size, as well as on the ligand. For example, AuNCs are used as catalysts in oxidation reaction. But depending on the size, different oxidation reactions are catalysed, since for some of them, it is necessary a larger band gap or a weaker thiol-gold bond. On the other hand, for the biolabeling or theranostic applications, the most important is the ligand and its compatibility with different organisms and cells.

Since the properties of AuNCs are directly related to their size, its precise control is an important feature. So, the synthesis of AuNCs has been widely studied, being divided into two strategies: top-down and bottom-up synthesis [3]. Top-down synthesis starts from bigger particles to obtain smaller ones, which is mainly done by etching with different ligands. Bottom-up synthesis, on the other hand, start with atomic precursors like gold salt using then a reduction agent. In the present work, only the bottom-up approach using thiol ligands is studied.

There are still two important issues due to the low stability of AuNCs: handling and storage. Different strategies have been employed to solve these issues. In the present work, the strategy is the encapsulation of AuNCs into polymer nanoparticles (PNPs). This strategy has been explored by different researchers with different goals. For catalysis, Yu's team developed AuNCs encapsulated in dendrimer-like micelles [16], while Miyamura and Kobayashi encapsulate the AuNCs into polystyrene through ''one-pot tandem

reaction'' [17]. Other used similar strategies to produce nanogels with AuNCs [8] or self-assembled peptides [11] for applications in the biological field. The polymerization techniques were mostly free radical polymerization. The techniques studied in the present work are miniemulsion polymerization and polymerization induced self-assembly (PISA).

Miniemulsion polymerization and PISA are dispersed polymerizations. This type of polymerization has been widely developed in the last decades thanks to its popularity in both academia and industry [18]. The overall advantages are good control of particle size, low viscosity (good temperature control), high yield of polymerization, high solids content, and good for environment [19].

Miniemulsion polymerization has been designed to overcome the limitations of emulsion polymerization in encapsulating hydrophobic components. It consists of a system of heterophases, generating monomer droplets between 50 and 500nm [18], with four main components: water, monomer, surfactant and co-stabilizer.

It starts with a two phases system (Figure 1): aqueous phase and monomer phase. First, the system is stirred creating an emulsion and then a shear force is applied through a homogenization process, generating small droplets. The nucleation occurs mainly in these droplets.

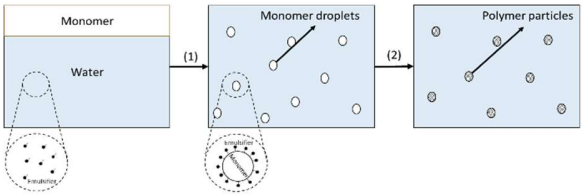

Figure 1. Miniemulsion polymerization according to nanoreactor's principle [18]: (1) sonication, (2) polymerization.

Efficient homogenization processes lead to smaller particles. On the other hand, the surfactant contributes to the droplet electrostatic stabilization avoiding coalescence during collision of droplets. The co-stabilizer, also known as hydrophobe, reduces the diffusion of monomer in the aqueous phase, avoiding Ostwald ripening. One of the most used costabilizer is hexadecane.

Inside the droplets, the polymerization proceeds as bulk polymerization, each droplet behaving like an individual nanoreactor [18, 20].

PISA is a quite recent technique. It consists in the self-assembly of a block copolymers with one-block part soluble and another insoluble in the solvent continuous phase during its synthesis [21]. The initial soluble block can be synthesized by different controlled radical polymerization (CRP) techniques. In this work, only reversible addition-fragmentation chain transfer polymerization (RAFT) was used.

RAFT results from the balance between active and dormant species through a chain transfer process [22].

PISA-RAFT starts with hydrophilic polymer living chains (macroCTA), and proceeds with the addition of monomer units, forming a hydrophobic second block (Figure 2). At a certain chain length, the polymer chain is no longer soluble in the water, leading to the self-assembly into sterically-stabilized micelles. Inside the micelles, the polymerization proceeds as bulk polymerization.

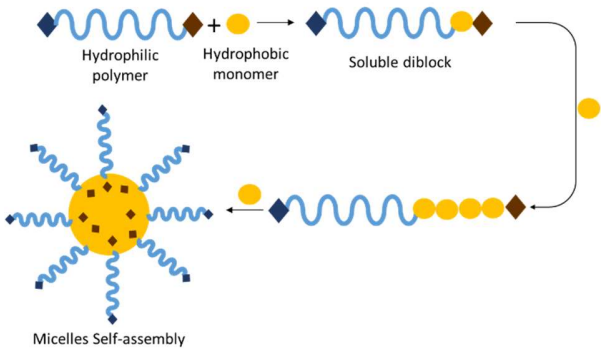

Figure 2. Principles of PISA via RAFT.

The main advantages of PISA -RAFT are its simplicity (one-pot process), reproducibility, lower number of purification and synthesis steps, wide range of functionalities and no use of surfactants. The core applications for polymer nanoparticles synthesized by PISA are drug delivery [19]. Since it is a new field, new applications are still being studied. Most of the studies, until the present, are about the morphology and properties control of particles [21].

2. Experimental

2.1. Materials

For the synthesis was used gold (III) chloride trihydrate ($HAuCl_4.3H_2O$, ≥99.9% trace metals basis, Sigma-Aldrich), 6-Mercaptohexnoic acid (MHA, 90%, Sigma-Aldrich), sodium hydroxide (NaOH, pure, EKA Pellets), hexadecyltrimethylammonium bromide (CTAB, 99+%, ACRÔS organics), absolute ethanol (EtOH, 99.8%, Sigma-Aldrich), toluene (99.5+% toluene ACS, Sigma-Aldrich), and sodium borohydride ($NaBH_4$, >98.5%, Sigma-Aldrich), styrene (Sty, Fluka), butyl methacrylate (BMA, 99%, Sigma-Aldrich), 1,3,5-trioxane (≥99%, Sigma-Aldrich), 4,4'-azobis(4-acide cyanopentanoique) (ACPA, Fluka, ≥98%) and sodium bicarbonate ($NaHCO_3$, Merck) were used without further purification. The deionized water used in the preparation of solutions and in some synthesis, was generated by a Millipore Milli-Q system (≥18 MΩcm, Merck). N-acryloyl morpholine (NAM, Sigma-Aldrich, 97%, distilled at 120°C and 10mmHg [19]), tert-butyl dithioenzoate (tBDB, synthesized according to Favier et al [23]), 1,4-dioxane (Sigma-Aldrich, ≥99%, distilled with $LiAlH_4$ at 110°C [19]), 2,2'-azobis(isobutyronitrile) (AIBN, Fluka, ≥98% (GC), recrystallized in ethanol [19]) and n-butyl acrylate (nBA, Sigma-Aldrich, ≥99%, distilled with hydroquinone at reduced pressure [19]), acetonitrile (Ficher, HPLC grade, distilled [19]), 1,4-butanediol diacrylate (BDDA, Aldrich, 90%, purified using an inhibitor remover column (Aldrich)) were used after purification.

2.2. AuNCs synthesis

Gold Nanoclusters with 6-mercaptohexanoic acid were synthesized according to reference [24], with minor modifications. The procedure is the dissolution of $HAuCl_4 \cdot 3H_2O$ (1eq.) to deionized water, to obtain a concentration of 6.50 mM. Then, the solution is placed in a bath at 27ºC with magnetic stirring. MHA is added to the solution followed by deionized water to obtain a concentration of 0.93 mM in $HAuCl_4 \cdot 3H_2O$. The colour change from yellow to orange and then colourless. To control pH, a solution of NaOH with 1.09 M (44.6 eq) is added, which turns the solution completely transparent. Lastly, a solution of $NaBH_4$ in water and NaOH ([NaOH]=0.22 M) is added dropwise. Depending on the amount of $NaBH_4$ and MHA, the solution acquires different colours, from brown to transparent. The reaction is left for 3h stirring at 27ºC.

The two AuNCs studied in detail have the following molar ratios:

- Au_{25}: MHA:Au=2.05 and $NaBH_4$:Au=2.19.
- Au_5 and Au_{11}: MHA:Au=6.00 and $NaBH_4$:Au=0.50.

A procedure from reference [24] was adapted to transfer AuNCs from water to the monomer or toluene. Firstly, for miniemulsion polymerization, a solution of CTAB in ethanol (0.1 M) is prepared. In the case of PISA, the solvent was 80% acetonitrile and 20% water in volume. The same volumes of AuNCs aqueous dispersion and CTAB solution are added. The ratio of styrene:Au added is 0.25 in volume. For the other monomers, it was 0.12, while in the case of toluene, the ratio is 1. The mixture is then stirred magnetically for 5 min. After that, the two phases start to separate and the AuNCs migrate to the organic phase.

2.3. Miniemulsion polymerization incorporating AuNCs

Miniemulsion polymerization incorporating the gold nanoclusters is done according the protocol from reference [25]. The stabilizer and initiator have to be altered in order to be compatible with the CTAB around the AuNCs.

First, a solution of CTAB in deionized water is prepared to have a concentration of 0.014 g of CTAB/g water. The dispersion of AuNCs in monomer (1 eq.) is placed in a bath at 30ºC with magnetic stirring. To this mixture of AuNCs in monomer, it was added hexadecane (1.06 eq.), DVB (0.35 eq.), AIBN (0.25 eq.) and the solution of CTAB (1.00 eq.) previously prepared. The reactional mixture was stirred at 30ºC for 30 min. Then the emulsion is sonicated, with 3 cycles with the parameters: output 3; duty cycle: 50% and timer: 6 min.
The mixture is then added to a three-necked 500 mL round-bottom reactor, equipped with argon inlet, condenser and mechanical stirring. The mixture is degassed for 30 min while stirring with constant velocity. After that time, the bath is turned on at 65ºC and the reaction is kept at this temperature with a low flow of argon for 8h.

2.4. RAFT polymerization

The RAFT polymerization is done following the procedure of a reference [19]. A solution of tBDB in dioxane with a concentration of 100 mg/L is prepared. Then, 1.784 mL of tBDB solution was

added to 10 mg of NAM in a 150 mL Schlenk tube. A solution of 10 mg/mL of AIBN in dioxane is prepared, and 1.393 mL of this are added to the mixture of tBDB and NAM. 540.2 mg of trioxane are added to the mixture as well as 23.329 mL of dioxane. Three cycles of degassing with freeze-pump-thaw are performed. After, with stirring at 1000 rpm and a temperature of 80°C, the Schlenk tube is immersed in the bath.
The polymer is then purified by precipitation with 800 mL of diethyl ether, being then filtrated. The polymer is dried through vacuum for 20h. The purification (elimination of solvent, monomer and other reagents) is verified by ^{1}H NMR.

2.5. PISA - RAFT

The PISA polymerization is conducted accordingly to reference [19]. A solution of 0.184 g of PNAM synthesized by RAFT [19] (RAFT1, M_n= 10 300 g/mol) and 0.902 mL of MilliQ water is prepared. 0.301 mL of a solution of ACPA (0.048 M) and $NaHCO_3$ (0.166 M) is added and transferred to the Schlenk tube and 1.203 mL of acetonitrile and 0.403 mL of nBA are added.
One of the following degassing methods was then performed:

1. 3 cycles of freeze-pump-thaw.
2. 30 min of argon flushing.
3. 30 min under argon with a condenser.

The tube is introduced in a oil bath at 80°C. The reaction, with stirring velocity between 1000 rpm and 1250 rpm, and the reaction is kept in this conditions for about 20h. During the reaction samples are withdrawn with a canula at different times to study the kinetics through NMR analysis.

2.6. PISA-RAFT incorporating AuNCs

Following the same protocol as in section 2.5, but adding 811 µL of organic phase with the AuNCs and 795 µL of acetonitrile.

2.7. Characterization methods

The TEM apparatus used to characterize the miniemulsion PNPs was Hitachi transmission electron microscope of model H-8100 with LaB6 filaments (Hitachi, Tokyo, Japan) and operated by Tânia Ribeiro. The accelerator voltage is 200 kV and the current is 20 µA. The images were acquired by the camera KeenView of Soft Imaging System, using the software iTEM.

The TEM apparatus used to characterize the PISA PNPs was Philips transmission electron microscope of model CM120, both for regular TEM and cryoTEM, and operated by Pierre Alcouffe. HR TEM apparatus used to characterize the AuNCs were JEOL2100F TEM, operated by Pierre Alcouffe. The accelerating voltage used for the observation was 200 kV.

The miniemulsion PNPs and PISA PNPs were analyzed using Zetasizer Nano ZS from Malvern Instruments (UK) from model ZEN3600 with the detectors 173°.

To analyse the absorption properties of the particles the apparatus used was an UV-660 UV-VIS Spectrophotometer from JASCO International (Tokyo, Japan) with a double monochromator and photomultiplier detector for high resolution. It was also used a microplate reader from BioTek using the software Gen5®.

To analyse the emission and excitation of the particles a Horiba Jobin Yvon Fluorolog 3-22 spectrofluorimeter with a xenox lamp of 450V was used. The software used was FluorEssence®.

The analysis using NMR was done at 298 K in an apparatus Spectro BRUKER AVANCE US+ 400MHz with a probe 5 mm BBFO+ Inverse detection multinuclear dual-broadband with Z-gradients.

The SEC-MALLS apparatus, operated by Agnès Crepet, was constituted by, first, an auto-injector Perkin Elmer, series 200 Autosampler injecting a volume of 1 mL. Secondly, there is a pump from Shimadzu model LC-20AD (1.0 mL/min). Then the column from Shimadzu mo-del CTO-20A working at 30°C. And, for last, the 2 sensors used were, first, the multi angle light scattering MiniDawn treos with 3 angles and, last, the refractometer from Shimadzu model RID-10A.

The GC apparatus is Agilent model 6890 Series, operated by Valentin Cinquin. The program starts at 40°C. Then with a ramp of 20°C/min, it goes to 300°C, staying at this temperature for 5min. The injector temperature is 240°C. The flow is 1 mL/min using ethanol, using a flame ionization detector (FID).

3. Results and Discussion

3.1. Characterization of $Au_{25}(MHA)_{18}$

In terms of visual aspect, the dispersion of $Au_{25}(MHA)_{18}$ is brown. The colour tends to get darker over time, but there is no sedimentation.

In terms of absorption (Figure 3a), two bands are identified (440 nm and 670 nm). They are the

characteristic bands of $Au_{25}(MHA)_{18}$ [26]. The bands are present for a period of 91 days, showing that the AuNCs are stable for about 3 months. In Figure 3a, the gold surface resonance plasmonic band of spherical particles is not present at 520 nm, which seems to indicate the absence of gold nanoparticles (AuNPs).

The emission spectra (Figure 3b) shows the presence of only one band at 810 nm for excitation wavelength from 440 nm to 680 nm. It shows that there is only one population.

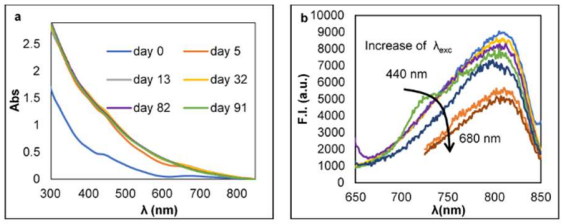

Figure 3. a) Absorption spectrum (top left – Au1) with time evolution: day 0 (blue), day 5 (orange), day 13 (grey), day 32 (yellow), day 82 (purple) and day 91 (green); c) Emission spectra (Au1) 13 days after synthesis with different λ_{exc}: 440nm (light blue), 480nm (yellow), 520nm (purple), 580nm (green), 620nm (dark blue), 670nm (orange) and 680nm (red).

HR TEM shows that the AuNCs are well dispersed and they don't show signs of aggregation (Figure 4a). The average size was (1.8±0.6) nm (Figure 4b), slightly higher than the literature values for other AuNCs with 25 atoms, which present values with less than 1.5 nm [27]. The lattice average size measured is (1.6 ±0.4) Å, which is similar to the literature [11]. It was calculated based in the HR TEM (Figure 4a), as the space between the atom lines in the AuNCs.

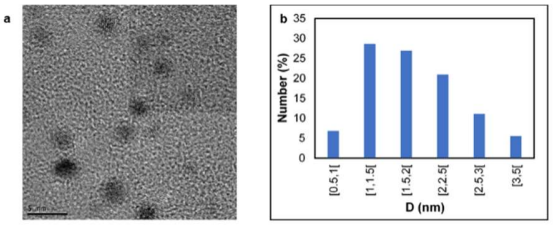

Figure 4. a) HR TEM image of $Au_{25}(MHA)_{18}$ (Au30). b) Size distribution of $Au_{25}(MHA)_{18}$ (Au31) by HR TEM.

3.2. Characterization of Au_5 and Au_{11}

By analysing two different factors in the AuNCs synthesis ($NaBH_4$:Au and MHA:Au molar ratios), smaller AuNCs were synthesized.

In terms of visual aspect, the dispersion is colourless. Over time, they tend to acquire a brown colour, indicative of an evolution in size over time.

It was not possible to visualize or measure the size of this AuNCs by HR TEM due to their small dimensions.

The absorption spectra do not show any band, which probably indicates the presence of multiple populations, i.e., there is AuNCs with more than one size.

The excitation spectrum shows a maximum at 320 nm and another at 440 nm (Figure 5a). The emission spectrum (Figure 5b) shows two bands: 380 nm and 500 nm, indicating the presence of two populations, confirmed by the results from the excitation.

Over time, the absorption spectra show one more band at 810 nm, showing that part of the AuNCs tend to evolve to Au_{25}, which are more stable.

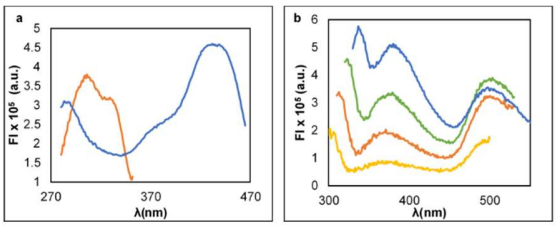

Figure 5. For molar ratios of MHA:Au=6.0 and $NaBH_4$:Au=0.5 (Au24): a) Excitation spectra with different λ_{em} : 380 nm (orange) and 495 nm (blue). b) Emission spectra with different λ_{exc}: 270 nm (yellow), 280 nm (orange), 290 nm (green) and 300 nm (blue).

The number of atoms was calculated with the Jellium model (equation 1), using the emission spectrum [28], were *N* is the number of atoms, E_F is the Fermi's energy and *Eg* is the band gap energy. The band at 380 nm, from the emission spectrum, corresponds to AuNCs with 5 atoms, while the one at 500 nm corresponds to 11 atoms.

$$E_g = \frac{E_F}{N^{\frac{1}{3}}} \qquad (1)$$

3.3. Miniemulsion polymerization incorporating AuNCs

The particles of polystyrene with AuNCs show a purple coloration, which seems to indicate the presence of AuNPs.

In the emission spectra, firstly, it is detected a band at 310 nm, which corresponds to the excimer from the phenyl groups of polystyrene particles [29]. To supress the excimer band, a filter was used, allowing to identify the band at 815 nm as the AuNCs band.

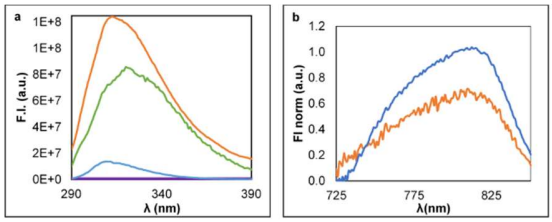

Figure 6. a) Emission spectrum with λ_{exc}=250nm and slits=14.7nm: AuNCs in aqueous phase (purple – Au1), PNPs of polystyrene with AuNCs in dispersion (blue – ME1), PNPs in pellets (orange – ME1) and polystyrene pellets (green). b) Emission spectra using λ_{exc}=380 nm (light blue), and λ_{exc}=650 nm (orange). Maximum intensity at λ_{em}=812 nm.

The particles size is measured by DLS, as (63±4) nm. The value is confirmed by TEM, (61±11) nm, showing round morphology.

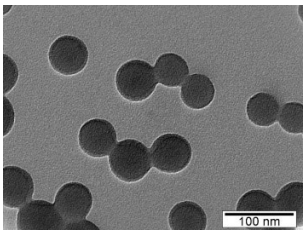

Figure 7. TEM image of PNPs of polystyrene with $Au_{25}(MHA)_{18}$

The final conversion was 70%, with a solid content of 18 %. It shows similar results to the adapted protocol [25].

To avoid the presence of the excimer, the polymerization was performed using butyl methacrylate (BMA). The polymerization proceeds in the presence of AuNCs, but a lower conversion was obtained (24%). The PBMA particles have (28±8) nm of diameter.

It was tested lowering pH from the PBMA particles dispersion. The AuNCs kept their properties, opposite to what happens when AuNCs are in aqueous dispersion. These results indicate that the AuNCs are inside the PBMA nanoparticles, opening good perspectives.

3.4. PISA incorporating AuNCs

Starting from an optimized PISA protocol using PNAM as macroCTA and butyl acrylate (BA) as hydrophobic monomer, the incorporation of AuNCs were achieved through the change and optimization of different parameters. The initial parameters were the ones in Table 1.

Table 1. Initial parameters of PISA.

Molar ratio		T (°C)	Time (h)
BA:PNAM	PNAM:ACPA		
157	2.5	80	20

PNAM was synthesized by RAFT, with a conversion of 80%, a M_n of 10 300 g mol^{-1} and a dispersity close to 1, as determined by SEC/MALLS.

First, the degassing method was optimized to minimize destabilising the $Au_{25}(MHA)_{18}$. Even though freeze-pump-thaw is the more efficient method, the chosen method was degassing under argon with an ice condenser above the liquid level. It minimizes the temperature changes and the destabilization by contact with air bubbles. The evaporation is also minimized when compared with argon flushing.

The phase transfer is optimized for $Au_{25}(MHA)_{18}$, using a solution of 100 mM of CTAB, in which the solvent is 80%(v) acetonitrile and 20%(v) water. It prevents the addition of new solvents to PISA - RAFT, since this could interfere with the monomer solubility, and consequently with the polymerization and self-assembly. The AuNCs in the organic phase (BA and acetonitrile) were studied by UV-Vis spectroscopy, TEM and HR TEM. The absorption bands of $Au_{25}(MHA)_{18}$ in organic phase are the same as in water, showing only that in the organic phase the $Au_{25}(MHA)_{18}$ concentration is higher (Figure 8 a). By TEM and HR TEM it was shown that $Au_{25}(MHA)_{18}$ are well dispersed, not being accumulated in interfaces or single areas. The size is also similar to the one measured for $Au_{25}(MHA)_{18}$ in water (1.6±0.4) nm (Figure 8 b) using the same techniques.

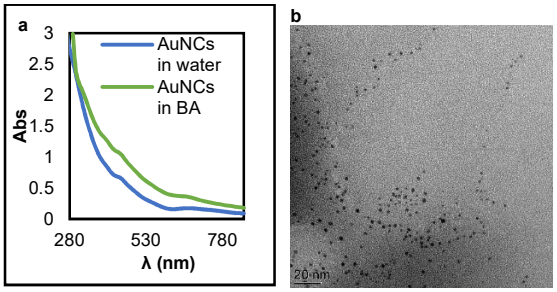

Figure 8. a) Absorption spectra of $Au_{25}(MHA)_{18}$ (Au40) in water (blue) and nBA and acetonitrile(green). b) TEM image of $Au_{25}(MHA)_{18}$ (Au41) in organic phase (nBA and acetonitrile).

The incorporation of AuNCs does not affect significantly the kinetics of PISA-RAFT, independently of the $Au_{25}(MHA)_{18}$ concentration. The size, on the other hand, is correlated with the $Au_{25}(MHA)_{18}$ concentration (Figure 9). The size tends to decrease with the increase of the $Au_{25}(MHA)_{18}$ concentration, since the concentration of CTAB increases too. CTAB is in excess when compared with MHA. This leads to the hypothesis that CTAB act in a similar manner to miniemulsion polymerization, stabilizing more the particles.

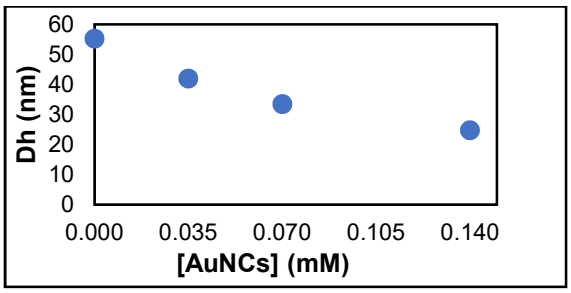

Figure 9. Evolution of hydrodynamic diameter with AuNCs concentration in the organic phase (PISA 8 to 11).

From the first synthesis of PISA-RAFT with AuNCs, it was noticed that after 20h at 80°C, there was no emission and the colour changed to purple. Both results seem to indicate the evolution from AuNCs to AuNPs. This idea is supported by the work of Chen and co-workers [30]. They study the sensitivity of $Au_{25}(MHA)_{18}$ upon exposure to temperatures higher than room temperature for different periods of time. Following that, we studied the behaviour of $Au_{25}(MHA)_{18}$ in water and in organic phase at 80°C for 3h and 65°C for 6h. After the 3h at 80°C, the absorption bands were no longer identifiable, especially in the organic phase due to the higher concentration (Figure 10 a and b). At 65°C after the 6h, the bands were less defined, which shows that there was already some degradation, but not as much as at 80°C after 3h. The absence of defined bands shows that different populations of AuNCs are present in solution, showing that temperature such as 80° C or 65°C for long period of time lead to degradation of AuNCs. It was also shown that the $Au_{25}(MHA)_{18}$ were stable for a longer period at 65°C.

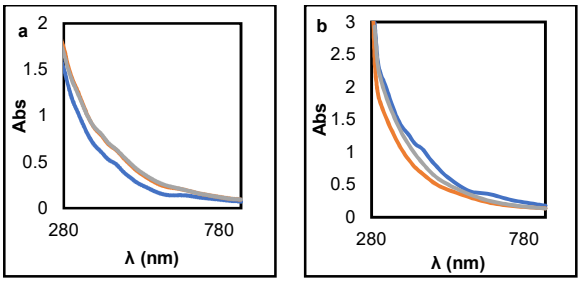

Figure 10. a) Absorption spectra of aqueous dispersion of AuNCs after being exposed to different temperatures (Au40). b) Absorption spectra of dispersion of AuNCs in nBA and acetonitrile after being exposed to different temperatures (Au40). The samples are only after synthesis (blue), after 6 h at 65 °C (orange) and after 80°C for 2h (grey).

PISA was studied at 65°C due to the stability of $Au_{25}(MHA)_{18}$ for a longer period at this temperature. Since it has a lower polymerization rate, due to the slower initiator decomposition, different ratios of PNAM: ACPA were studied by changing the concentration of ACPA (initiator). It was shown that by decreasing the molar ratio PNAM: ACPA (increase of ACPA concentration), the rate of polymerization increases, but there is loss of the polymerization control. The increase in the ACPA concentration leads to an increase in the radical concentration. It leads to an increase of termination processes and of the number of BA homopolymer-chains, produced without a macroCTA. A compromise was established between polymerization rate and control and $Au_{25}(MHA)_{18}$ stability. Two polymerizations were studied in detail in the presence of AuNCs:

1. At 80°C, using PNAM:ACPA=2.5, for 2h;
2. At 65°C, using PNAM:ACPA=1.25, for 6h.

In terms of kinetics, the polymerization at 80°C had faster rate of polymerization as expected (Figure 11). The final conversion for (1) and (2) is similar: about 45%. After stopping the polymerization, two phases were evident in both synthesis due to the partial conversion of BA. For (1) there was a top dark brown phase with the unreacted BA and $Au_{25}(MHA)_{18}$, and a bottom

orange phase with a tone of brown, and some sedimentation of brown particles in the bottom. For (2) both phases were brown, being the top phase only slightly darker, without any sedimentation.

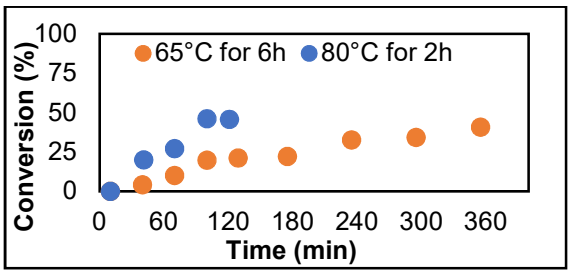

Figure 11. Kinetics of PISA-RAFT with AuNCs at 80°C for 2h and PNAM:ACPA=2.5 (PISA 15) and at 65°C for 6h and PNAM:ACPA=1.25 (PISA 19).

In terms of size, the particles from both synthesis have similar size and morphology (Table 2). But in the synthesis (2) there is loss of control of polymerization, since two populations were detected by DLS: one with about 28 nm and another one at 166±21 nm, but representing only 0.3% in number.

Table 2. Comparison between average results by TEM and by DLS for PISA at 80°C (1) (PISA 15) and at 65°C (2) (PISA 19).

	TEM			DLS
	D core (nm)	Shell thickness (nm)	D (nm)	D_h (nm)
With AuNCs @ 80°C	12±2	4±1	20	26.8±0.4
With AuNCs @ 65°C	9±3	4±1	17	28.3±0.3

The top phase of (1) was studied by HR TEM (Figure 12) in order to analyse the size and dispersion of the $Au_{25}(MHA)_{18}$ in BA after 2h at 80°C with strong stirring. The $Au_{25}(MHA)_{18}$ were well dispersed in the organic phase (Figure 12), and the average diameter of $Au_{25}(MHA)_{18}$ was (1.8±0.5) nm, similar to the value measured before the polymerization. The $Au_{25}(MHA)_{18}$ does not seem to suffer any change in size during the first 2h of PISA at 80°C, as opposite of the observed after 3h by UV-Vis absorption.

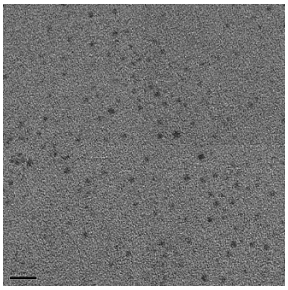

Figure 12. TEM image of $Au_{25}(MHA)_{18}$ organic phase (top phase) of PISA at 2h at 80°C with high stirring velocity (PISA 15).

The optical properties of the bottom phase of both syntheses were analysed by fluorescence emission. Both synthesis show fluorescence emission at 820 nm, but (2) has higher maximum intensity (Figure 13).

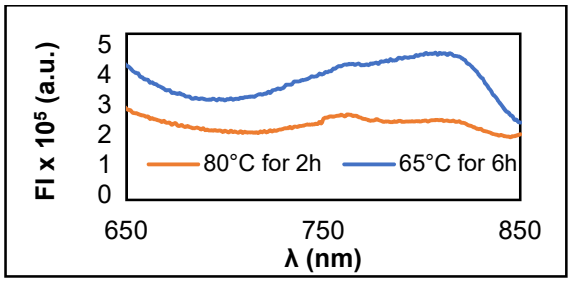

Figure 13. Fluorescent emission spectra of PISA with AuNCs at 80°C for 2h and PNAM:ACPA=2.5 (PISA 15) and at 65°C for 6h and PNAM:ACPA=1.25 (PISA 19), with λ_{exc}=450nm.

The fine localization of the $Au_{25}(MHA)_{18}$ in the PNPs could not be precisely determined since it was not possible to visualize both ($Au_{25}(MHA)_{18}$ and PNPs) at the same time by TEM, cryoTEM or HR TEM. While TEM and cryoTEM did not allow to visualize the $Au_{25}(MHA)_{18}$ due to their resolution and low contrast, HR TEM does not allow to visualize PNPs due to the applied voltage. This could be the object of further optimization in the future.

We also performed PISA-RAFT with in the presence of crosslinker. It could increase the stability of $Au_{25}(MHA)_{18}$, by decreasing the mobility of $Au_{25}(MHA)_{18}$. It does not interfere with the kinetics or size of the PISA-RAFT PNPs ((31±2) nm). Further studies are needed to confirm the role of crosslinker in PISA with $Au_{25}(MHA)_{18}$.

By both techniques, hybrid particles were obtained. Since they are based in different mechanisms, it is difficult to compare the two

techniques. While, with miniemulsion there is the presence of toxic hexadecane, in PISA-RAFT acetonitrile is the solvent and it is also toxic.

Conclusions

The objective of the project was to stabilize AuNCs through incorporation into polymer nanoparticles (PNPs) by miniemulsion polymerization and PISA-RAFT.

Two different synthesis of AuNCs were studied: $Au_{25}(MHA)_{18}$, and Au_5/Au_{11}. The $Au_{25}(MHA)_{18}$ have a higher stability, emitting in the biological ''transparency window'' considering wavelength range. The Au_5/Au_{11} emit between 380 nm and 500 nm, which can be applied in the imaging field. They have lower stability, which can be improved by a deeper study of the synthesis conditions.

The encapsulation of $Au_{25}(MHA)_{18}$ by miniemulsion polymerization was successfully achieved with this robust polymerization technique, obtaining particles with about 50 nm. Some parameters can still be improved, such as the polymerization time to reduce the $Au_{25}(MHA)_{18}$ degradation with temperature.

For PISA-RAFT with $Au_{25}(MHA)_{18}$ polymer-stabilized PNPs below 30 nm were obtained. The parameters were successfully optimized to allow the PNPs formation without major degradation of $Au_{25}(MHA)_{18}$. To conclude about which are the better conditions, further investigation is needed since this results from a compromise between polymerization control and $Au_{25}(MHA)_{18}$ stability.

In both cases, miniemulsion polymerization and PISA-RAFT, it was possible to obtain PNPs in the presence of $Au_{25}(MHA)_{18}$.

References

1. Mingos, D.M.P., *Gold Clusters, Colloids and Nanoparticles I*2014: Springer International Publishing.
2. Jin, R.C., *Quantum sized, thiolate-protected gold nanoclusters.* Nanoscale, 2010. **2**(3): p. 343-362.
3. S. G., B., *Síntesis, caracterización y propiedades fluorescentes de clústeres cuánticos subnanométricos*, in *Departamento de Química-Física*2012, Universidade de Santiago de Compostela: Facultad de Química. p. 173.
4. Zheng, Y., et al., *Recent advances in biomedical applications of fluorescent gold nanoclusters.* Advances in Colloid and Interface Science, 2017. **242**: p. 1-16.
5. Buceta, D., et al., *Metallic Clusters: Theoretical Background, Properties and Synthesis in Microemulsions.* Catalysts, 2014. **4**(4): p. 356-374.
6. Snow, A.W., M.G. Ancona, and D. Park, *Nanodimensionally Driven Analyte Response Reversal in Gold Nanocluster Chemiresistor Sensing.* Langmuir, 2012. **28**(44): p. 15438-15443.
7. Ancona, M.G., et al., *Analyte kinetics in a nanocluster-based chemiresistor: A case study.* Sensors and Actuators B-Chemical, 2013. **177**: p. 936-946.
8. Chen, Y., et al., *Near-Infrared Emitting Gold Cluster–Poly(acrylic acid) Hybrid Nanogels.* ACS Macro Letters, 2014. **3**(1): p. 74-76.
9. Li, J.J., et al., *Nanomaterial-based activatable imaging probes: from design to biological applications.* Chemical Society Reviews, 2015. **44**(21): p. 7855-7880.
10. Yu, Y., et al., *Scalable and Precise Synthesis of Thiolated Au10-12, Au-15, Au-18, and Au-25 Nanoclusters via pH Controlled CO Reduction.* Chemistry of Materials, 2013. **25**(6): p. 946-952.
11. Zhang, W., et al., *Supramolecular Self-Assembly Bioinspired Synthesis of Luminescent Gold Nanocluster-Embedded Peptide Nanofibers for Temperature Sensing and Cellular Imaging.* Bioconjugate Chemistry, 2017. **28**(9): p. 2224-2229.
12. Yahia-Ammar, A., et al., *Self-Assembled Gold Nanoclusters for Bright Fluorescence Imaging and Enhanced Drug Delivery.* Acs Nano, 2016. **10**(2): p. 2591-2599.
13. Chen, D., et al., *Amphiphilic Polymeric Nanocarriers with Luminescent Gold Nanoclusters for Concurrent Bioimaging and Controlled Drug Release.* Advanced Functional Materials, 2013. **23**(35): p. 4324-4331.
14. Sahoo, A.K., et al., *Simultaneous RGB Emitting Au Nanoclusters in Chitosan Nanoparticles for Anticancer Gene Theranostics.* Acs Applied Materials & Interfaces, 2014. **6**(1): p. 712-724.
15. Wu, X.T., et al., *Multifunctional spherical gold nanocluster aggregate@polyacrylic acid@mesoporous silica nanoparticles for combined cancer dual-modal imaging and chemo-therapy.* Journal of Materials Chemistry B, 2015. **3**(12): p. 2421-2425.

16. Yu, Y.Y., et al., *Dendrimer-like core cross-linked micelle stabilized ultra-small gold nanoclusters as a robust catalyst for aerobic oxidation of alpha-hydroxy ketones in water.* Green Chemistry, 2016. **18**(12): p. 3647-3655.
17. Miyamura, H. and S. Kobayashi, *Tandem Oxidative Processes Catalyzed by Polymer-Incarcerated Multimetallic Nanoclusters with Molecular Oxygen.* Accounts of Chemical Research, 2014. **47**(4): p. 1054-1066.
18. Landfester, K., *Miniemulsions for Nanoparticle Synthesis*, in *Colloid Chemistry II*, M. Antonietti, Editor 2003, Springer Berlin Heidelberg: Berlin, Heidelberg. p. 75-123.
19. Duret, D., *Développement de sondes polymères fluorescentes à propriétés de ciblage améliorées pour des applications en imagerie cellulaire et en oncologie*, in *INSA Lyon*2016.
20. Asua, J.M., *Miniemulsion polymerization.* Progress in Polymer Science, 2002. **27**(7): p. 1283-1346.
21. Warren, N.J. and S.P. Armes, *Polymerization-Induced Self-Assembly of Block Copolymer Nano-objects via RAFT Aqueous Dispersion Polymerization.* Journal of the American Chemical Society, 2014. **136**(29): p. 10174-10185.
22. Favier, A., M.T. Charreyre, and C. Pichot, *A detailed kinetic study of the RAFT polymerization of a bi-substituted acrylamide derivative: influence of experimental parameters.* Polymer, 2004. **45**(26): p. 8661-8674.
23. Favier, A., et al., *Study of the RAFT polymerization of a water-soluble bisubstituted acrylamide derivative. 1. Influence of the dithioester structure.* Macromolecules, 2002. **35**(22): p. 8271-8280.
24. Yao, Q.F., et al., *Introducing Amphiphilicity to Noble Metal Nanoclusters via Phase-Transfer Driven Ion-Pairing Reaction.* Journal of the American Chemical Society, 2015. **137**(5): p. 2128-2136.
25. Augusto, V., et al., *Oxygen-proof fluorescence temperature sensing with pristine C-70 encapsulated in polymer nanoparticles.* Journal of Materials Chemistry, 2010. **20**(6): p. 1192-1197.
26. Yuan, X., et al., *Balancing the Rate of Cluster Growth and Etching for Gram-Scale Synthesis of Thiolate- Protected Au25 Nanoclusters with Atomic Precision.* Angewandte Chemie-International Edition, 2014. **53**(18): p. 4623-4627.
27. Yuan, X., et al., *Insights into the effect of surface ligands on the optical properties of thiolated Au25 nanoclusters.* Chemical Communications, 2016. **52**(30): p. 5234-5237.
28. Zheng, J., C.W. Zhang, and R.M. Dickson, *Highly fluorescent, water-soluble, size-tunable gold quantum dots.* Physical Review Letters, 2004. **93**(7).
29. Kuo, A., *Fluorescence Resulting from π-stacking in Polystyrene Solutions.* ChemM, 2011.
30. Chen, T., et al., *Heating or Cooling: Temperature Effects on the Synthesis of Atomically Precise Gold Nanoclusters.* The Journal of Physical Chemistry C, 2017. **121**(20): p. 10743-10751.